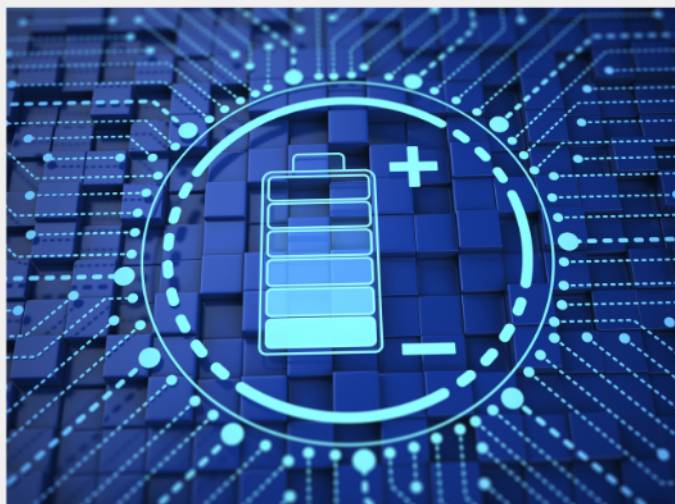# Exploring the possibilities of increasing energy density and efficiency in rechargeable batteries

Download this complimentary article collection

The exponential rise in the need for better, more efficient power sources has sparked an incredible amount of research into batteries. A primary focus of research has been increasing the energy density of batteries, as it allows for lighter, more portable storage of energy. Lithium-ion batteries, for example, have a much higher energy density than conventional lead-acid batteries and can be used for various purposes, such as in electric vehicles.

This article collection provides a comprehensive list of references for new methods and technologies for increasing the energy density of batteries.

Ω Metrohm

WILEY

RESEARCH ARTICLE

ADVANCED
FUNCTIONAL
MATERIALS

www.afm-journal.de

Check for updates

Impact of RbF and NaF Postdeposition Treatments on Charge Carrier Transport and Recombination in Ga-Graded Cu(In,Ga)Se$_2$ Solar Cells

Yu-Han Chang, Romain Carron, Mario Ochoa, Ayodhya N. Tiwari, James R. Durrant,* and Ludmilla Steier*

Two key strategies for enhancing the efficiency of Cu(In,Ga)Se$_2$ solar cells are the bandgap gradient across the absorber and the incorporation of alkali atoms. The combined incorporation of Na and Rb into the absorber has brought large efficiency gains compared to Na-containing or alkali-free layers. Here, transient absorption spectroscopy is employed to study the effect of NaF or combined NaF+RbF postdeposition treatments (PDT) on minority carrier dynamics in different excitation volumes of typical composition-graded Cu(In,Ga)Se$_2$ solar cells. Electron lifetimes are found to be highly dependent on the film composition and morphology, varying from tens of nanoseconds in the energy notch to only ≈100 ps in the Ga-rich region near the Mo-back contact. NaF PDT improves recombination lifetimes by a factor of 2–2.5 in all regions of the absorber, whereas the effectiveness of the RbF PDT is found to decrease for higher Ga-concentrations. Electron mobility measured in the absorber region with large grains is promoted by both alkali PDTs. The data suggest that NaF PDT passivates shallow defect states (Urbach tail) throughout the Cu(In,Ga)Se$_2$ film (including the interior of large grains), whereas the additional RbF PDT is effective at grain boundary surfaces (predominantly in regions with medium to low Ga-concentrations).

1. Introduction

Alkali atom incorporation in Cu(In,Ga)Se$_2$ (CIGSe) absorbers along with an engineered bandgap-gradient profile (obtained through varying the [Ga]/([Ga]+[In]) (GGI) ratio) has proven to be essential for achieving high device efficiencies.[1,2] Historically, alkali atom incorporation of Na (and to an extent K) ions stemmed from the soda-lime glass (SLG) substrate, especially for high-temperature CIGSe deposition processes.[1] It is also possible and very effective to introduce alkali atoms by controlled alkali post-deposition treatments (PDT) after the CIGSe deposition, which do not significantly influence CIGSe grain growth or the GGI profile compared to other alkali incorporation methods.[3] CIGSe solar cells generally show higher device efficiencies with light NaF[4] and especially heavy alkali KF,[5] RbF, or CsF treatments.[6]

Among all the alkali PDTs, the effect of Na has been studied most intensively. It is generally observed that the open-circuit voltage (V_{OC}), and fill factor (FF) increase with an optimal Na incorporation.[7–10] Several studies correlated the increase in V_{OC} and FF with the increased p-type character of the Na-treated CIGSe absorber.[7,9,11,12] Other studies showed that the increase in V_{OC} and FF can result from the passivation of non-radiative recombination centers at grain boundaries (GBs), evidenced by several atom probe tomography studies showing Na accumulation predominantly at GBs compared to grain interiors (GIs).[13–20] Transient optical studies correlated increased charge carrier lifetime with optimal Na atom incorporation[21–23] Eid et al. utilized ultrafast pump-probe reflectance spectroscopy to study Ga-graded CIGSe devices with different thicknesses of NaF (incorporated prior to selenization) and found a 1.5-fold increase in minority carrier lifetime in samples with higher Na concentrations which was correlated with higher device performance[10,21] However, owing to the variation in the composition gradient with different Na concentrations in this experiment design, the role of Na atoms could not be clearly identified. Lee et al. detected a ≈fivefold prolonged charge carrier lifetime on CIGSe (GGI = 0.14) grown on SLG compared to reference films grown on borosilicate glass, concluding that the addition of Na atoms prohibits the formation of defect states at the CdS/CIGSe junction and hence increases carrier lifetime.[22] Though the study did not address the correlation between defect states and GBs, a smaller grain size

Dr. Y.-H. Chang, Prof. J. R. Durrant, Dr. L. Steier
Department of Chemistry
Centre for Processable Electronics
Imperial College London
White City Campus, London W12 0BZ, UK
E-mail: j.durrant@imperial.ac.uk; l.steier@imperial.ac.uk

Dr. R. Carron, Dr. M. Ochoa, Prof. A. N. Tiwari
Laboratory for Thin Films and Photovoltaics
Empa—Swiss Federal Laboratories for Materials Science and Technology
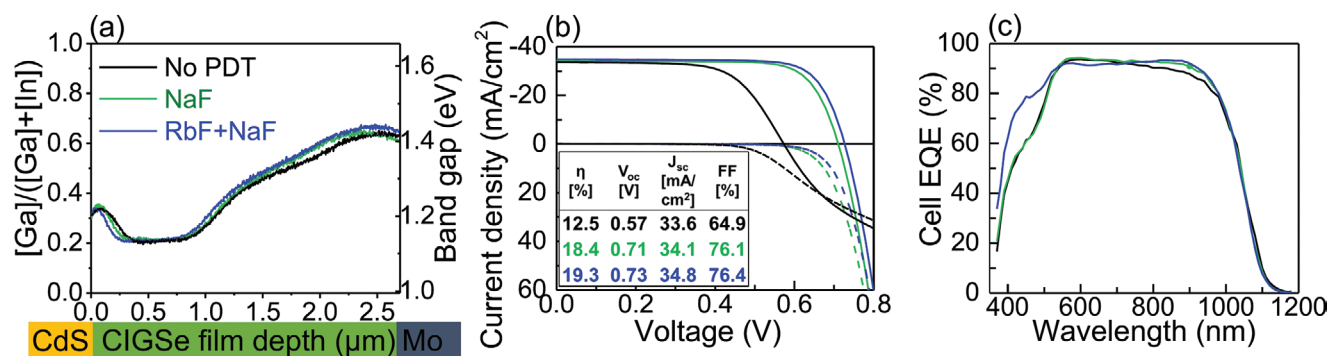Überlandstrasse 129, Dübendorf CH-8600, Switzerland

The ORCID identification number(s) for the author(s) of this article can be found under https://doi.org/10.1002/adfm.202103663.

**ADVANCED
SCIENCE NEWS**

www.advancedsciencenews.com

**ADVANCED
FUNCTIONAL
MATERIALS**

www.afm-journal.de

Figure 1. Device characteristics of alkali-free (black), NaF (green), and RbF+NaF treated (blue) Ga-graded CIGSe solar cells. a) Secondary ion mass spectrometry depth profiles, illustrating the increasing [Ga]/([Ga]+[In]) (GGI) ratio (and corresponding bandgap) along the CIGSe absorber towards CdS and Mo sides (with especially high GGI ratios towards the Mo side) leaving a region with minimum GGI ratio in between (termed "energy notch" throughout this paper) in all three devices. b) J-V characteristics under standard test conditions (100 mW cm^{-2}, 1 sun), and c) external quantum efficiency. Note that the SIMS depth profile in (a) and J-V characteristic in (b) of the RbF+NaF PDT device are the same as in our previous publication which we required to establish the model for carrier recombination and diffusion in typical Ga-graded CIGSe solar cells.[37]

was observed in the borosilicate CIGSe device. Using time-resolved photoluminescence spectroscopy, Jarzembowski et al. showed that the rear surface recombination velocity in a CIGSe thin film with NaF PDT (with GGI = 0.4) is reduced threefold compared to the one without any PDT,[23] indicating Na atoms affect the recombination at the Mo/CIGSe back interface.

Following this large body of research on NaF PDTs, more recent studies have focused on the combined incorporation of light and heavy alkali atoms, for example, NaF+RbF. At the front interface, RbF PDT has been shown to cause Cu-depletion and a Rb enrichment.[24] Similar to the KF PDT, treatment with the heavier Rb atoms allows for the deposition of a thinner CdS layer which increases cell J_{SC}.[5] In CIS, Cu-deficiency has been calculated to induce Cd atoms to occupy Cu or Cu-vacancy sites during the CdS chemical bath deposition process,[25] and indeed Cd has been observed to diffuse around 10 nm into CIGS films.[26] It was proposed that Cd$_{Cu}$ donors lead to electronic inversion of the CIGSe surface resulting in the formation of a p-n homojunction which improves device efficiency.[5] Another reason for the enhanced J_{SC} could result from Rb atoms accumulating at the front interface forming secondary phases: Taguchi et al. demonstrated the formation of a thin RbInSe$_2$ layer at the CdS/CIGSe (GGI = ≈0.2–0.3) interface via transmission electron microscopy,[27] which is assumed to create an additional valence band offset and reduce recombination at this interface[28,29] In the bulk of the Na-containing CIGS, it was found that the diffusion of Rb atoms via GBs is strongly enhanced due to the presence of Na atoms, whilst the diffusion via GIs is severely hampered.[30] A displacement of Na from GBs by Rb[5,6] was also found in atom probe topography and secondary ion mass spectroscopy studies.[30–32] It was suggested that Rb may slow down non-radiative recombination in the bulk, possibly associated with a reduction in the density of defect states in the bulk.[33] Several studies have observed the charge carrier lifetime in Ga-graded CIGSe absorbers to increase by a factor of 4 after RbF PDT.[34–36] However, these studies only addressed the influence of Rb near the CdS/CIGSe interface, which typically exhibits GGI ratios <0.5, and the effect of Rb in different GGI regions of Ga-graded CIGSe absorber layers remains largely undetermined.
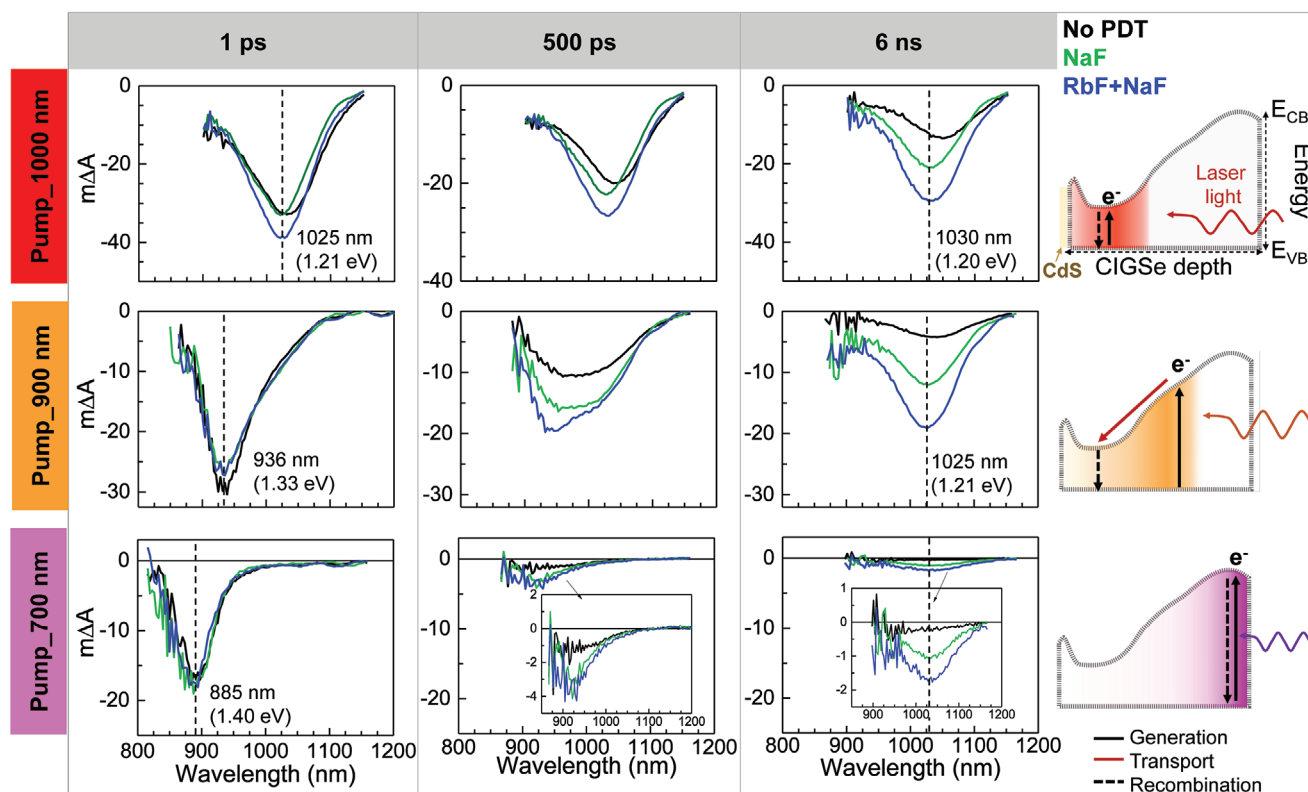
In the study herein we focus on the impact of Na and Rb PDTs on charge carrier recombination kinetics in Ga-graded CIGSe solar cells. Utilizing ultrafast (ps-ns) transient absorption spectroscopy (TAS) measurements coupled to a kinetic model we established previously,[37] we demonstrate differing impacts of these PDTs on recombination losses in regions with high and low Ga-content and link these kinetics to device performance. Importantly, we can disentangle the impact of the alkali treatment from one of the GGI profiles since our samples are fabricated with an identical GGI profile which allows us to compare the impact of the alkali PDTs across the full absorber depth.

2. Results

Three CIGSe absorbers were characterized in this study, with an identically engineered Ga-gradient across the absorber depth as shown in **Figure 1**a. The layers were deposited on SLG substrates coated with an alkali diffusion barrier and Mo back contact. One layer was kept alkali-free (termed "No PDT"), whereas the other layers were subject to in situ NaF or NaF+RbF PDT after absorber deposition. The layers were processed into devices with typical device structures (AZO/i-ZnO/CdS/CIGSe/Mo). Figure 1b shows the J-V characteristics of such "No PDT", "NaF PDT", and "RbF+NaF PDT" CIGSe devices. The efficiency enhancement in devices with alkali PDT results from a large V_{OC} improvement (25 and 28% relative to the No PDT after NaF PDT and NaF+RbF PDT, respectively).

Figure 1c shows the external quantum efficiency (EQE) spectra. Compared to the untreated and NaF treated devices, the RbF+NaF PDT device presented an increased EQE value in the 400–500 nm range, due to the thinner CdS layer used (25 nm instead of 50 nm).[5,24,38] The thinner CdS layer also slightly affected the EQE shape in the visible due to modified interference fringes. Compared to the NaF-treated device, the No PDT device (with the same CdS thickness) showed a significantly lower EQE response in the 800–1000 nm region, suggesting a carrier collection issue in the No PDT device.

To understand this collection issue and the V_{OC} loss in the device, the charge carrier dynamics on ps-ns timescales in

**ADVANCED
SCIENCE NEWS**

www.advancedsciencenews.com

**ADVANCED
FUNCTIONAL
MATERIALS**

www.afm-journal.de

Figure 2. Femtosecond transient absorption (fs-TA) measurements showing spectral snapshots at 1 ps, 500 ps and 6 ns after excitation (columns) with 1000, 900, and 700 nm pump laser light (rows) of No PDT (black traces), NaF PDT (green), and RbF+NaF PDT (blue) samples. Samples were excited from the peeled-off Mo side (indicated by the wavy arrows in the specific row colors red, orange, and purple). The schematics on the right-hand side represent the carrier generation volumes in the CIGSe film as shaded areas (see Figure S1, Supporting Information). The laser excitation power density corresponds to 7×10^{13} photons cm^{-2} per pulse.

these CIGSe solar cells were investigated (**Figure 2**). The samples from the delaminated Mo/SLG substrate side were excited using pump wavelengths of 1000, 900, and 700 nm which allowed to track charge carriers generated at different depths in the Ga-graded CIGS film. The schematic in the last column of Figure 2 shows the excitation volumes for each pump wavelength, based on optical TMM calculations of the charge carrier generation profiles (see Figure S1, Supporting Information).

Overlaying the bandgap profile of the CIGSe layer with the simulated charge carrier generation profiles for each pump wavelength (Figure S1, Supporting Information), the 1 ps photobleach peak energy was assigned in a Ga-graded RbF+NaF PDT CIGSe layer to the ground state bleach of the corresponding band edge absorption, as detailed in our previous work.[37] The 1 ps spectra of the alkali-treated and untreated CIGSe films show no significant difference in spectral shape or intensity, as expected from their nearly identical GGI profiles (Figure 1a). As such, the 1 ps photobleach peaks were assigned in all 3 samples to carriers generated i) in the energy notch by excitation with 1000 nm, ii) at intermediate bandgap energy by excitation with 900 nm, and iii) close to the (removed) Mo back contact by excitation with 700 nm laser light. In this last case, the 1 ps bleach peak was centered at about 885 nm well below the pump excitation energy, limited by the highest bandgap in the absorber. Note that in the 900 nm excitation case, the curves deviated from the usual Gaussian-shape and showed an asymmetric edge towards lower energies because

the charge carrier generation profile extends into the energy notch (Figure S1, Supporting Information). It was further noted that in the 1000 nm excitation case, a slightly more redshifted photobleach peak energy was observed in the No PDT sample (1040 nm) compared to the PDT samples (1025 nm). The redshift was slightly more than expected from the EQE curves (about 5 meV difference). This difference could be related to minor sample inhomogeneities or a slight change in the occupancy of states near the band edge upon PDT. This latter hypothesis of occupying or removing shallow donor states near the CB edge by the Na PDT would be consistent with the observed increase in p-type character upon alkali atom PDT treatment.[11,30,35,39]

With 1000 nm excitation (Figure 2, top row), the amplitude and peak position of the photobleach were very similar until at least ≈500 ps. At later times when the signal significantly decayed, a slight shift in peak position was observed from 1025 to 1030 nm for alkali-treated samples and from 1040 to 1050 nm for the No PDT sample. The excitation volume accessed with 900 nm laser excitation (Figure 2, middle row) presented a gradient in GGI ratio ranging from 0.2 to 0.5, and consisted of large grains (see Figure S2, Supporting Information). By 500 ps, the photobleach has lost amplitude and a red-shifted bleach grows in. By 6 ns, only the red-shifted photobleach peak centered at 1025 nm for the PDT samples and 1040 nm for the No PDT sample persisted, that is, identical to the peak energy obtained with 1000 nm excitation at 1 ps. The final photobleach
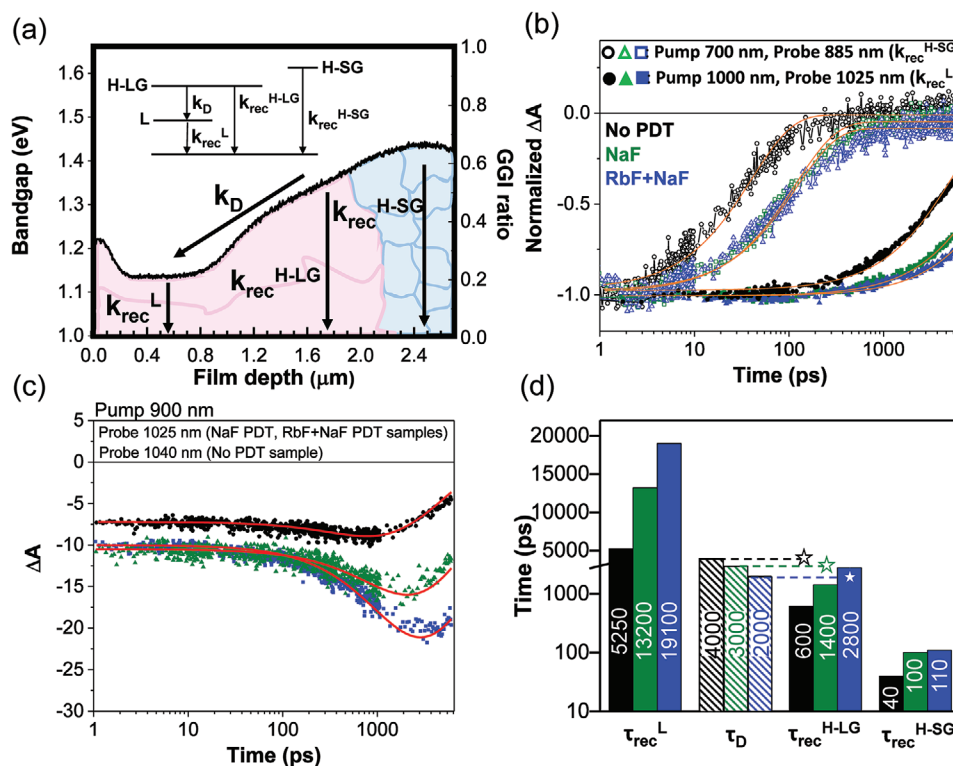
Figure 3. a) Schematic of the model for electron dynamics in the Ga-graded CIGSe absorber layer. The GGI ratio and the corresponding energy bandgap are based on the SIMS result of RbF+NaF PDT sample (Figure 1a). k_{rec}^L, k_{rec}^{H-LG}, and k_{rec}^{H-SG} denote the decay constants for charge recombination in the energy notch (names as L), in the high bandgap regions exhibiting large grains (named as H-LG) and small grains (named as H-SG) respectively. b) Transient absorption decay kinetics using 700 nm laser excitation probed at 885 nm and using 1000 nm laser excitation probed at 1025 nm. c) TA kinetics using probed at 1025 (NaF PDT and RbF+NaF PDT) or 1040 nm wavelength (No PDT). The red lines show the fitting results. The laser excitation power density corresponds to 7×10^{13} photons cm^{-2}. d) Time constants of the TAS decays in the energy notch (τ_{rec}^L), in the H-LG (τ_{rec}^{H-LG}), and the H-SG (τ_{rec}^{H-SG}) regions and the corresponding drift time constant (τ_D). The stars indicate the competition between charge recombination and drift.

signal amplitude in the RbF+NaF PDT sample was about 4 times larger than in the No PDT sample. Upon excitation with 700 nm (Figure 2, bottom row), a rapid photobleach decay was seen in all 3 samples (more than half of its original amplitude decays by 500 ps) and a very small red-shifted signal centered at 1025 nm for the PDT samples was left by 6 ns.

The red-shift in photobleach (from the initial excitation volume to ≈1025 nm) was assigned to a drift-diffusion process (with a time constant $\tau_D = 1/k_D$, with k_D being the rate constant of the drift-diffusion process) of charge carriers from their initial excitation volume to the energy notch region.[37] This assignment was based on the previously established kinetic model as shown in **Figure 3**a. The model is based on four decay constants describing minority carrier movement and recombination in the Ga-graded CIGSe absorber layer which was divided into three excitation volumes (excited with 1000, 900, and 700 nm). The decay constants were k_{rec}^L for electron recombination in the energy notch (GGI ≈ 0.2), k_{rec}^{H-LG} and k_D for recombination and drift in large grains with a GGI gradient (here varying from 0.5 to 0.2), and k_{rec}^{H-SG} for electron recombination in small grains with GGI > 0.6 (see SEM image in Figure S2, Supporting Information). This multi-level kinetic model was discussed in more detail elsewhere.[37]

The kinetics of carriers in the small grain region with a GGI ratio of ≈0.6 are given in Figure 3b (pump 700 nm, probe

880 nm) along with the kinetics of carriers excited in the energy notch (pump 1000 nm, probe 1025 nm). Fitting their decays with a single exponential function, recombination times τ_{rec}^{H-SG} = 40, 100, and 110 ps were obtained in the high-GGI/small grain (H-SG) region, and τ_{rec}^L = 5.3, 13.2, and 19.1 ns in the energy notch region of No PDT, NaF PDT, and RbF+NaF PDT samples, respectively.

The kinetics of carriers arriving from the GGI-graded excitation volume (which was accessed with 900 nm excitation) in the energy notch were probed with 1025 nm (Figure 3c). The rise of the 1025 nm signal holds information on both, the recombination of those carriers initially excited in the GGI-graded volume and their drift-diffusion process to the energy notch as derived in the previous work on this model.[37] Fitting of the kinetics (see Figures S3–S5, Table S1, Supporting Information, and previous work for further details) in Figure 3c and the spectra shown in Figure 2, recombination times τ_{rec}^{H-LG} ≈600, 1200, and 2200 ps and transfer times τ_D ≈ 4000, 2800, and 1900 ps could be decoupled in No PDT, NaF PDT, and RbF+NaF PDT samples, respectively. The transfer times correspond to twice as high mobilities in the RbF+NaF treated device compared to the untreated one. The resulting four time constants (τ_{rec}^L, τ_{rec}^{H-LG}, τ_D, and τ_{rec}^{H-SG}) for all three samples are plotted in comparison in Figure 3d and are discussed below.

**ADVANCED
SCIENCE NEWS**

www.advancedsciencenews.com

**ADVANCED
FUNCTIONAL
MATERIALS**

www.afm-journal.de

Note that experiments with 700 nm laser excitation were also carried out from both, the Mo side and the AZO side (See Figure S6, Supporting Information) showing fully consistent results from both sides: the RbF+NaF PDT sample shows the most charge carriers transferred, and charge carriers are also most long-lived, followed by the NaF Na PDT. The No PDT sample shows the fastest decay.

3. Discussion

Independent of the PDTs, we observe a general trend of faster recombination in CIGSe with higher GGI ratios. This finding aligns well with the reported correlation of smaller V_{OC} deficit for smaller energy notch GGI ratios observed in record-efficiency devices.[40] However, we observe that the effectiveness of each PDT varies across the CIGSe absorber layer. In the following, we compare and discuss the observed differences in recombination times and mobilities of electrons in the energy notch, H-LG, and H-SG regions among No PDT, NaF PDT, and NaF+RbF PDT samples.

3.1. Comparison of NaF PDT versus No PDT

Na has been suggested to passivate (i.e., remove) compensating donor defects such as the Se vacancy (V_{Se}) or the In on Cu anti-site (In_{Cu}) in the GIs and GBs leading to the observed increase in p-type character in CIGS.[41,42] Furthermore, a recent study from Siebentritt et al.[33] reported on a reduction in the Urbach energy of the NaF PDT CIGSe device (that was fabricated analogous to our samples) and proposed the passivation of tail states in the bulk by NaF PDT. From our results, by comparing recombination time constants with and without Na (τ_{rec}^{L}, τ_{rec}^{H-LG}, and τ_{rec}^{H-SG}), the incorporation of Na improves the charge carrier lifetime by a factor of 2–2.5, independent of the local GGI ratio. If Na ions were effective predominantly at GBs, we would expect to see a proportional change in electron lifetime in excitation volumes with higher GB area (i.e., H-SG). However, we do not seem to observe this proportional increase and would tend to argue that Na has a more significant effect in the bulk/GI. This is corroborated by a 1.5-fold increase in electron mobility in the NaF treated sample (11.2 cm^{2}V^{-1}s^{-1} in the No PDT, 16.3 cm^{2}V^{-1}s^{-1} in the NaF PDT sample) which we calculate from the electron drift time constant in the H-LG region where far fewer GBs are visible compared to the H-SG volume. We also observe a ≈17 meV blue shift in the photobleach peak wavelength in the energy notch region in our alkali-treated samples (1025 nm in PDT samples vs 1040 nm in No PDT). Despite sample inhomogeneities and a 5 meV bandgap difference (taken from EQE data), it is likely that the difference in Urbach energies between the PDT and the No PDT samples attributes to this photobleach peak difference. These two observations support the effectiveness of NaF in GIs where deeper levels of shallow defect states are passivated throughout the grain thereby decreasing recombination and enhancing mobility. We note, however, that our results do not exclude simultaneous GB defect passivation as

observed recently[43] but rather suggest a significant role of defect passivation in GIs by NaF.

3.2. Comparison of RbF+NaF PDT versus NaF PDT

As shown in Figure 3d, the charge carrier lifetime in the energy notch of the combined NaF+RbF PDT sample is 1.4 times longer compared to the NaF sample. This observation aligns well with other studies that suggest Rb passivating additional recombination centers in the space charge region,[34–36] which lies within the range of the energy notch region. Furthermore, we see a ≈1.9-fold improvement in carrier lifetime and ≈1.5 times faster charge transport in the bandgap-graded H-LG region. These observations show that Rb acts even slightly stronger along the bandgap gradient where more GBs are visible ($\tau_{rec}^{H-LG(RbF+NaF)}/\tau_{rec}^{H-LG(NaF)} \approx 1.9$) compared to the energy notch $\tau_{rec}^{L(RbF+NaF)}/\tau_{rec}^{L(NaF)} \approx 1.4$). This is in agreement with reports showing Rb segregation at GBs.[32,44,45] Even though the formation of a RbInSe$_2$ surface layer[27] is found to segregate at the CdS/CIGSe (GGI = 0.2–0.3) surface, we are aware that the amount of Rb atoms segregated inside the CIGSe absorber layer (low ppm range or below) may not be sufficient to form extended RbInSe$_2$ phases. However, this does not preclude the significant impact on charge transport, by local band bending and/or electrical fields induced by fixed charges.

In contrast to the increase in electron lifetime observed with RbF PDT in the energy notch region, RbF PDT barely increases electron lifetime in the small grain/high GGI (H-SG) region (only 1.1-fold increase) despite its higher GB area. Interestingly, a study by Ishizuka et al. demonstrated a negligible impact of RbF PDT on the device performance of a CGSe solar cell.[46] Since we do observe a significant improvement of electron lifetime upon NaF treatment in the H-SG region, the lack of further improvement upon NaF+RbF might indeed support Ishizuka's observation and hint towards an ineffective Rb passivation in CIGSe with high GGI ratios.

3.3. Linking Charge Carrier Dynamics to Device Performance

Drift ($\tau_D \approx 1.9$ ns) slightly outcompetes recombination ($\tau_{rec}^{H-LG} \approx 2.2$ ns, $\tau_D/\tau_{rec}^{H-LG} = 0.9$) in the NaF+RbF PDT sample, whilst the other samples both show faster recombination ($\tau_D/\tau_{rec}^{H-LG} = 2.3$ and 6.5 for NaF and No PDT, respectively). The competing recombination and drift mechanisms in the H-LG volume control the yield of minority carriers in the energy notch (Figure 3c), and ultimately the photovoltage (and current) in the solar cell device. Indeed, both alkali treatments (NaF and combined NaF+RbF) enhance charge collection from the graded CIGSe volume (Figure 3c); this is also visible in the EQE data in the 750–1000 nm region (Figure 1c). This enhanced charge collection can explain the significant difference in V_{OC} of alkali-treated and untreated devices (>140 mV difference) and the slight difference in V_{OC} between the alkali-treated devices.

The H-SG region shows recombination times on the order of ≈100 ps in all three devices and hence drift-diffusion of carriers from this volume is not observed even in the PDT samples. Here, other strategies such as an adjustment of the GGI

ratio and/or morphological control towards the growth of larger grains on the Mo substrate might hold more promise than aiming for improvements with alkali PDTs. It should be noted that the surface recombination at the air-exposed back surface may also contribute to the short-lived charge carriers from the H-SG region.[37] This may in part be caused by surface oxidation in the H-SG region induced by air exposure. Surface recombination is also likely to be severe in typical devices with a Mo back contact.[47] Therefore, in a typical functional device, significant charge carrier transport from the H-SG region to the energy notch is not expected either.

4. Conclusion

Utilizing TAS, we have investigated identically Ga-graded CIGSe layers with 3 different post-deposition processing conditions (No PDT, NaF, and NaF+RbF PDT). Segmenting the CIGSe films in 3 regions, namely the energy notch region (GGI ≈0.2), a bandgap graded region (GGI 0.2–0.5, "H-LG"), and a region with GGI>0.6 and small grain size ("H-SG"), we observe the varying influence of the PDTs on electron lifetimes and mobilities. The NaF PDT treatment increases the minority carrier lifetime ≈2–2.5-fold in all absorber regions. Analysis of TAS spectra in the energy notch region, suggests that NaF PDT passivates shallow defects (i.e., tail states below the conduction band minimum) most likely in the bulk of CIGSe grains (though surface defect passivation is not excluded). Additional RbF PDT further improves the minority carrier lifetime in the energy notch (1.4-fold) and Ga-graded H-LG region (≈twofold), whereas the improvement is negligible in the small grain/high GGI (H-SG) region. We conclude that the effectiveness of the RbF PDT is strongly dependent on the GGI ratio and is most effective for low GGI (i.e., <0.5) compositions. Further experiments are required to investigate the positive impact of Rb in low GGI CIGSe in more detail and shine light on the role of RbInSe$_2$ formation for as small Rb concentrations as present in our devices to understand the impact of Rb on local band bending and band offsets.

Furthermore, both NaF and the combined NaF+RbF PDTs significantly improve electron transport kinetics from the Ga-graded H-LG region to the energy notch, likely causing the improved EQE response in the 750–1000 nm region and larger V_{OC} in the PDT devices. Strategies to further improve CIGSe solar cell efficiency would need to focus on the H-SG region where an adjustment of the GGI ratio, morphological control towards the growth of larger grains on the Mo substrate, and the use of suitable charge selective layers might hold more promise than aiming for further improvements with alkali PDTs.

Supporting Information

Supporting Information is available from the Wiley Online Library or from the author.

Acknowledgements

Conflict of Interest

The authors declare no conflict of interest.

Data Availability Statement

The data supporting the findings of this study are openly available in Zenodo at http://doi.org/10.5281/zenodo.4698954 under the Creative Commons Attribution 4.0 International license.

Keywords

[1] J. Hedstrom, H. Ohlsen, M. Bodegard, A. Klyner, L. Stolt, D. Hariskos, M. Ruckh, H. W. Schock, in *Conf. Rec. Twenty Third IEEE Photovolt. Spec. Conf. - 1993 (Cat. No.93CH3283-9)*, Louisville, KY, USA **1993**, pp. 364–371.

[2] M. A. Contreras, B. Egaas, P. Dippo, J. Webb, J. Granata, K. Ramanathan, S. Asher, A. Swartzlander, R. Noufi, in *Conf. Rec. Twenty Sixth IEEE Photovolt. Spec. Conf. - 1997*, Anaheim, CA, USA **1997**, pp. 359–362.

[3] D. Colombara, K. Conley, M. Malitckaya, H.-P. Komsa, M. J. Puska, *J. Mater. Chem. A* **2020**, *8*, 6471.

[4] D. Rudmann, D. Brémaud, A. F. Da Cunha, G. Bilger, A. Strohm, M. Kaelin, H. Zogg, A. N. Tiwari, *Thin Solid Films* **2005**, *480–481*, 55.

[5] A. Chirilă, P. Reinhard, F. Pianezzi, P. Bloesch, A. R. Uhl, C. Fella, L. Kranz, D. Keller, C. Gretener, H. Hagendorfer, D. Jaeger, R. Erni, S. Nishiwaki, S. Buecheler, A. N. Tiwari, *Nat. Mater.* **2013**, *12*, 1107.

[6] P. Jackson, R. Wuerz, D. Hariskos, E. Lotter, W. Witte, M. Powalla, *Phys. Status Solidi RRL* **2016**, *10*, 583.

[7] D. Rudmann, A. F. Da Cunha, M. Kaelin, F. Kurdesau, H. Zogg, A. N. Tiwari, G. Bilger, *Appl. Phys. Lett.* **2004**, *84*, 1129.

[8] L. Kronik, D. Cahen, H. W. Schock, *Adv. Mater.* **1998**, *10*, 31.

[9] S. H. Wei, S. B. Zhang, A. Zunger, *J. Appl. Phys.* **1999**, *85*, 7214.

[10] J. Eid, H. Liang, I. Gereige, S. Lee, J.V Duren, *Prog. Photovoltaics* **2015**, *23*, 269.

[11] T. Nakada, D. Iga, H. Ohbo, A. Kunioka, *Jpn. J. Appl. Phys.* **1997**, *36*, 732.

[12] R. Kimura, T. Nakada, P. Fons, A. Yamada, S. Niki, T. Matsuzawa, K. Takahashi, A. Kunioka, *Sol. Energy Mater. Sol. Cells* **2001**, *67*, 289.

[13] O. Cojocaru-Mirédin, P. P. Choi, D. Abou-Ras, S. S. Schmidt, R. Caballero, D. Raabe, *IEEE J. Photovoltaics* **2011**, *1*, 207.

[14] A. Laemmle, R. Wuerz, T. Schwarz, O. Cojocaru-Mirédin, P.-P. Choi, M. Powalla, *J. Appl. Phys.* **2014**, *115*, 154501.

**ADVANCED
SCIENCE NEWS**

www.advancedsciencenews.com

**ADVANCED
FUNCTIONAL
MATERIALS**

www.afm-journal.de

[15] E. Cadel, N. Barreau, J. Kessler, P. Pareige, *Acta Mater.* **2010**, *58*, 2634.

[16] P. P. Choi, O. Cojocaru-Mirédin, R. Wuerz, D. Raabe, *J. Appl. Phys.* **2011**, *110*, 124513.

[17] D. Braunger, D. Hariskos, G. Bilger, U. Rau, H. W. Schock, *Thin Solid Films* **2000**, *361*, 161.

[18] D. W. Niles, M. Al-Jassim, K. Ramanathan, *J. Vac. Sci. Technol., A* **1999**, *17*, 291.

[19] M. Raghuwanshi, E. Cadel, S. Duguay, L. Arzel, N. Barreau, P. Pareige, *Prog. Photovoltaics* **2017**, *25*, 367.

[20] D. Azulay, D. Abou-Ras, I. Popov, I. Balberg, O. Millo, *Phys. Status Solidi RRL* **2016**, *10*, 448.

[21] J. Eid, A. Usman, I. Gereige, J. Van Duren, V. Lyssenko, K. Leo, O. F. Mohammed, *Sol. Energy Mater. Sol. Cells* **2015**, *140*, 33.

[22] W. J. Lee, D. H. Cho, J. H. Wi, W. S. Han, Y. D. Chung, J. Park, J. M. Bae, M. H. Cho, *J. Phys. Chem. C* **2015**, *119*, 20231.

[23] E. Jarzembowski, F. Syrowatka, K. Kaufmann, W. Fränzel, T. Hölscher, R. Scheer, *Appl. Phys. Lett.* **2015**, *107*, 051601.

[24] E. Avancini, R. Carron, T. P. Weiss, C. Andres, M. Bü, C. Schreiner, R. Figi, Y. E. Romanyuk, S. Buecheler, A. N. Tiwari, *Chem. Mater.* **2017**, *29*, 9695.

[25] J. Kiss, T. Gruhn, G. Roma, C. Felser, *J. Phys. Chem. C* **2013**, *117*, 10892.

[26] T. Nakada, A. Kunioka, *Appl. Phys. Lett.* **1999**, *74*, 2444.

[27] N. Taguchi, S. Tanaka, S. Ishizuka, *Appl. Phys. Lett.* **2018**, *113*, 113903.

[28] D. Hauschild, D. Kreikemeyer-Lorenzo, P. Jackson, T. M. Friedlmeier, D. Hariskos, F. Reinert, M. Powalla, C. Heske, L. Weinhardt, *ACS Energy Lett.* **2017**, *2*, 2383.

[29] F. Pianezzi, P. Reinhard, A. Chirilă, B. Bissig, S. Nishiwaki, S. Buecheler, A. N. Tiwari, *Phys. Chem. Chem. Phys.* **2014**, *16*, 8843.

[30] R. Wuerz, W. Hempel, P. Jackson, *J. Appl. Phys.* **2018**, *124*, 165305.

[31] M. Raghuwanshi, E. Cadel, P. Pareige, S. Duguay, F. Couzinie-Devy, L. Arzel, N. Barreau, *Appl. Phys. Lett.* **2014**, *105*, 013902.

[32] A. Vilalta-Clemente, M. Raghuwanshi, S. Duguay, C. Castro, E. Cadel, P. Pareige, P. Jackson, R. Wuerz, D. Hariskos, W. Witte, *Appl. Phys. Lett.* **2018**, *112*, 103105.

[33] S. Siebentritt, E. Avancini, M. Bär, J. Bombsch, E. Bourgeois, S. Buecheler, R. Carron, C. Castro, S. Duguay, R. Félix, E. Handick, D. Hariskos, V. Havu, P. Jackson, H. Komsa, T. Kunze, M. Malitckaya, R. Menozzi, M. Nesladek, N. Nicoara, M. Puska, M. Raghuwanshi, P. Pareige, S. Sadewasser, G. Sozzi, A. N. Tiwari, S. Ueda, A. Vilalta-Clemente, T. P. Weiss, F. Werner, R. G. Wilks, W. Witte, M. H. Wolter, *Adv. Energy Mater.* **2020**, *10*, 1903752.

[34] T. Feurer, F. Fu, T. P. Weiss, E. Avancini, J. Löckinger, S. Buecheler, A. N. Tiwari, *Thin Solid Films* **2019**, *670*, 34.

[35] S. Karki, P. Paul, G. Rajan, B. Belfore, D. Poudel, A. Rockett, E. Danilov, F. Castellano, A. Arehart, S. Marsillac, *IEEE J. Photovoltaics* **2019**, *9*, 313.

[36] M. D. Heinemann, T. Kodalle, C. Hages, M. Klupsch, D. Greiner, L. Korte, S. Levcenco, T. Unold, R. Schlatmann, C. A. Kaufmann, *EPJ Photovoltaics* **2018**, *9*, 9.

[37] Y. Chang, R. Carron, M. Ochoa, C. Bozal-Ginesta, A. N. Tiwari, J. R. Durrant, L. Steier, *Adv. Energy Mater.* **2021**, *11*, 2003446.

[38] P. Reinhard, B. Bissig, F. Pianezzi, E. Avancini, H. Hagendorfer, D. Keller, P. Fuchs, M. Döbeli, C. Vigo, P. Crivelli, S. Nishiwaki, S. Buecheler, A. N. Tiwari, *Chem. Mater.* **2015**, *27*, 5755.

[39] Y. Sun, S. Lin, W. Li, S. Cheng, Y. Zhang, Y. Liu, W. Liu, *Engineering* **2017**, *3*, 452.

[40] M. Nakamura, K. Yamaguchi, Y. Kimoto, Y. Yasaki, T. Kato, H. Sugimoto, *IEEE J. Photovoltaics* **2019**, *9*, 1863.

[41] D. J. Schroeder, A. A. Rockett, *J. Appl. Phys.* **1997**, *82*, 4982.

[42] A. Rockett, *Thin Solid Films* **2005**, *480*, 2.

[43] M. Raghuwanshi, R. Wuerz, O. Cojocaru-Mirédin, *Adv. Funct. Mater.* **2020**, *30*, 2001046.

[44] P. Schöppe, S. Schönherr, P. Jackson, R. Wuerz, W. Wisniewski, M. Ritzer, M. Zapf, A. Johannes, C. S. Schnohr, C. Ronning, *ACS Appl. Mater. Interfaces* **2018**, *10*, 40592.

[45] P. Schöppe, S. Schönherr, R. Wuerz, W. Wisniewski, G. Martínez-Criado, M. Ritzer, K. Ritter, C. Ronning, C. S. Schnohr, *Nano Energy* **2017**, *42*, 307.

[46] S. Ishizuka, N. Taguchi, J. Nishinaga, Y. Kamikawa, S. Tanaka, H. Shibata, *J. Phys. Chem. C* **2018**, *122*, 3809.

[47] T. P. Weiss, B. Bissig, T. Feurer, R. Carron, S. Buecheler, A. N. Tiwari, *Sci. Rep.* **2019**, *9*, 5385.